JOURNAL OF GEOPHYSICAL RESEARCH, VOL. 115, A01209, doi:10.1029/2009JA014553, 2010



# Multispacecraft observation of electron pitch angle distributions in magnetotail reconnection

Rongsheng Wang,[1,2] Quanming Lu,[1,2] Can Huang,[1] and Shui Wang[1]

Received 10 June 2009; revised 29 August 2009; accepted 2 October 2009; published 23 January 2010.

[1] In this paper, we present Cluster observations of a magnetotail reconnection event without the presence of an obvious guide magnetic field and analyze electron pitch angle distributions in the vicinity of the X line and the outflow region, respectively. In the vicinity of the X line, at lower energies the distributions are highly anisotropic (field-aligned bidirectional anisotropic), while at higher energies, the electrons are observed to flow away from the X line along the magnetic field lines. The electron distributions change largely in the outflow region. At the edge of the outflow region, at lower energies, the electrons flow toward the X line, while the electrons at higher energies are directed away from the X line. When the satellites approach the center of the current sheet, at lower energies, the electrons have field-aligned bidirectional distributions, while at higher energies, the electron distributions are isotropic. The generation mechanisms of such distributions are explained by following typical electron trajectories in the electric and magnetic fields of magnetic reconnection, which are obtained in two-dimensional particle-in-cell simulations. It is shown that the observed high-energy electrons directed away from the X line both in the vicinity of the X line and in the outflow region are due to the acceleration by the reconnection electric field near the X line, and the field-aligned bidirectional distributions at lower energies are caused by the effects of the magnetic mirror in the reconnection site. The isotropic distributions at higher energies in the outflow region are the results of the electron stochastic motions when their gyroradii are comparable to the curvature radii of the magnetic field lines.

**Citation:** Wang, R., Q. Lu, C. Huang, and S. Wang (2010), Multispacecraft observation of electron pitch angle distributions in magnetotail reconnection, *J. Geophys. Res.*, *115*, A01209, doi:10.1029/2009JA014553.

## 1. Introduction

[2] Magnetic reconnection is a fundamental plasma process by which magnetic energy is rapidly converted into plasma energy, and it is also accompanied by magnetic topological changes [*Vasyliunas*, 1975; *Biskamp*, 2000; *Priest and Forbes*, 2000]. Magnetic reconnection is believed to be the major driving mechanism for many explosive phenomena in space and laboratory plasma, such as solar flares [*Giovanelli*, 1946; *Tsuneta et al.*, 1992], substorms in the Earth's magnetosphere [*Nishida*, 1978; *McPherron et al.*, 1987; *Ge and Russell*, 2006], and disruptions in laboratory fusion experiments [*Wesson*, 1997]. Since the first theoretical model for magnetic reconnection was proposed by *Sweet* [1958] and *Parker* [1957] more than 50 years ago, numerous theoretical and observational articles have been published along this line [*Birn et al.*, 2001; *Hesse et al.*, 2001; *Shay et al.*, 2001; *Wang et al.*, 2001; *Øieroset et al.*, 2001, 2002; *Nagai et al.*, 2001, 2003; *Pritchett and Coroniti*, 2004; *Zong et al.*, 2004; *Fu et al.*, 2006; *Cao et al.*, 2006; *Wei et al.*, 2007; *Xiao et al.*, 2007; *Drake et al.*, 2008; *Sergeev et al.*, 2008]. The fast rate of collisionless reconnection is considered to be determined by ion-scale Hall effects in the ion diffusion region [*Birn et al.*, 2001; *Shay et al.*, 2001; *Ma and Bhattacharjee*, 2001], which results from the decoupled motions of ions and electrons. At this scale length, the electrons are magnetized and frozen in the magnetic field lines, while the motions of ions are demagnetized. However, recent observations both in the magnetotail and during solar flares indicate that energetic electrons are one of the most important signatures in magnetic reconnection. In solar flares, X-rays are thought to be generated by energetic electrons in magnetic reconnection [*Lin and Hudson*, 1976; *Miller et al.*, 1997]. In the Earth's magnetotail, there have been a few direct measurements of energetic electrons associated with magnetic reconnection [*Øieroset et al.*, 2002; *Imada et al.*, 2007; *Retino et al.*, 2008; *Wang et al.*, 2008; *Chen et al.*, 2008a]. In the ion diffusion region, the outflow speed of the electrons is much larger than the Alfvén speed [*Pritchett*, 2001; *Drake et al.*, 2008]. The energetic electrons are considered to be accelerated near the X line when their motions are demagnetized, which gives rise to the off-diagonal electron pressure term and electron inertial term in the generalized Ohm's law. These terms are found to be the main cause of the reconnection electric field near

[1]Chinese Academy of Sciences Key Laboratory of Basic Plasma Physics, School of Earth and Space Sciences, University of Science and Technology of China, Hefei, China.
[2]State Key Laboratory of Space Weather, Chinese Academy of Sciences, Beijing, China.


0148-0227/10/2009JA014553$09.00

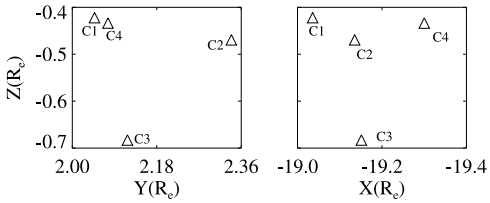


**Figure 1.** Positions of the Cluster spacecraft at 0755 UT on 10 September 2001 are shown in GSM coordinates. The GSM system has its *x* axis from the Earth to the Sun. The *y* axis is defined to be perpendicular to the Earth's magnetic dipole. The positive *z* axis is chosen to be in the same sense as the northern magnetic pole.

the X point [*Vasyliunas*, 1975; *Cai and Lee*, 1997; *Hesse and Winske*, 1998; *Pritchett*, 2001; *Kuznetsova et al.*, 2001; *Scudder et al.*, 2002; *Wan and Lapenta*, 2008]. Therefore, electron dynamics plays an important role in magnetic reconnection.

[3] Electron dynamics in collisionless magnetic reconnection has been previously studied using test particle calculations [*Speiser*, 1965; *Deeg et al.*, 1991; *Litvinenko*, 1996] and particle-in-cell (PIC) simulations [*Hoshino et al.*, 2001; *Hesse et al.*, 2001; *Pritchett and Coroniti*, 2004; *Fu et al.*, 2006; *Pritchett*, 2006a, 2006b; *Drake et al.*, 2008; *Wan et al.*, 2008]. The energetic electrons are accelerated mainly by the reconnection electric field in the vicinity of the X line. When there is no guide field, the electrons may be reflected back and enter the acceleration region several times before they leave the vicinity of the X line. When there is a guide field, although the reconnection electric field becomes smaller, the electrons may still be accelerated to higher energy by staying in the vicinity of the X line for a longer time because of the gyromotions of the electrons in the guide field [*Litvinenko*, 1996; *Fu et al.*, 2006]. *Chen et al.* [2008b] investigated electron distributions in an extended electron current sheet and its adjacent magnetic island with PIC simulations and compared them to Cluster observations. Electron dynamics has also been investigated with satellite observations [*Øieroset et al.*, 2001, 2002; *Nagai et al.*, 2001, 2003; *Wang et al.*, 2008]. *Øieroset et al.* [2001, 2002] reported a reconnection event with an obvious guide magnetic field in the deep magnetotail. During the process of the Wind spacecraft crossing the diffusion region from the earthward side to the tailward side, near the boundary between the plasma sheet and the lobe in the Southern Hemisphere, a low-energy (<300 eV) electron beam aligned with the magnetic field and directed toward the X line was observed just before the flow reversal. The same reconnection event has also been studied by *Egedal et al.* [2005], and it is found that near the center of the diffusion region, the electron pitch angle distributions with energies from 15.2 eV to 6 keV display peaks at 0° and 180° and minima at 90° (field-aligned bidirectional distributions), while the electron distributions become nearly isotropic at energies higher than 6 keV. Such distributions near the center of the diffusion region are attributed to the existence of a strong electrostatic potential, and some of the electrons are trapped by such potential. The electron distributions in the outflow region were also measured by Geotail and Wind spacecraft in the magnetotail [*Fujimoto et al.*, 1997; *Nagai et al.*, 2001, 2003; *Manapat et al.*, 2006] and by Cluster in the magnetotail [*Alexeev et al.*, 2005; *Asnes et al.*, 2008] and magnetopause [*Retino et al.*, 2006]. Hot and cold electrons, which flow away and toward the X line, respectively, are observed in this region.

[4] On 10 September 2001, Cluster observed a reconnection event in the Earth's magnetotail, and the satellites were moving from tailward to earthward of the reconnection site. Different from the reconnection event observed by Wind in the deep magnetotail [*Øieroset et al.*, 2001, 2002; *Egedal et al.*, 2005], there is no obvious observed guide field during this event. The spacecraft fortuitously measured the electron pitch angle distributions at different locations (in the vicinity of the X line and the outflow region). In this paper, we report the observational results of the reconnection event on 10 September and then analyze the generation mechanisms of such electron pitch angle distributions by following typical electron trajectories in the electric and magnetic fields of the reconnection, which are obtained in 2-D PIC simulations.

## 2. Cluster Observations

### 2.1. Overview

[5] In this paper, we report Cluster [*Escoubet et al.*, 2001] observations of the reconnection event during the interval 0748–0804 UT on 10 September 2001. During that interval, Cluster was located in the magnetotail plasma sheet, approximately 19 $R_E$ from the Earth, and it was moving from tailward to earthward of the reconnection site. Figure 1 shows the location of Cluster at 0755 UT on 10 September 2001 in the GSM coordinate system. Unless specified, we use GSM for the discussion throughout this paper. Cluster was located around $X = -19$, $Y = 2$, and $Z = 0R_E$. C1 (C3) was the northernmost (southernmost) spacecraft. We use measurements from several instruments on board Cluster. Magnetic field data are taken from the fluxgate magnetometer [*Balogh et al.*, 2001], which measures the three components of the low-frequency magnetic field. Ion plasma data are obtained from the ion Composition and Distribution Function analyzer (CODIF) instrument, which is part of the Cluster Ion Spectrometry (CIS) experiment [*Rème et al.*, 2001]. Low- to middle-energy electron data are taken from the Plasma Electron and Current Experiment (PEACE) instrument [*Johnstone*, 1997]. The PEACE instrument has two sensor heads, a low-energy electron analyzer and a high-energy electron analyzer (HEEA), which are mounted on opposite sides of the spacecraft. In this study, we use the pitch angle distribution data from PEACE-HEEA. The available energy range during the interest time interval is from about 40 eV to 8 keV.

[6] Figure 2 shows an overview of the Cluster observations from 0748 to 0804 UT with 4 s spin resolution. Figures 2a–2g show plasma proton density, the three components of the magnetic field, the *x* component of proton flow velocity, energy-time diagrams of ions (observed by C1), and energetic electron fluxes (observed by C1). Note that during this interval, C2 does not have the data on proton density and proton flow velocity. At the beginning of the interval shown in Figure 2, the satellites C1, C2, and C4 have positive $B_x$, while $B_x$ observed by C3 is almost zero.

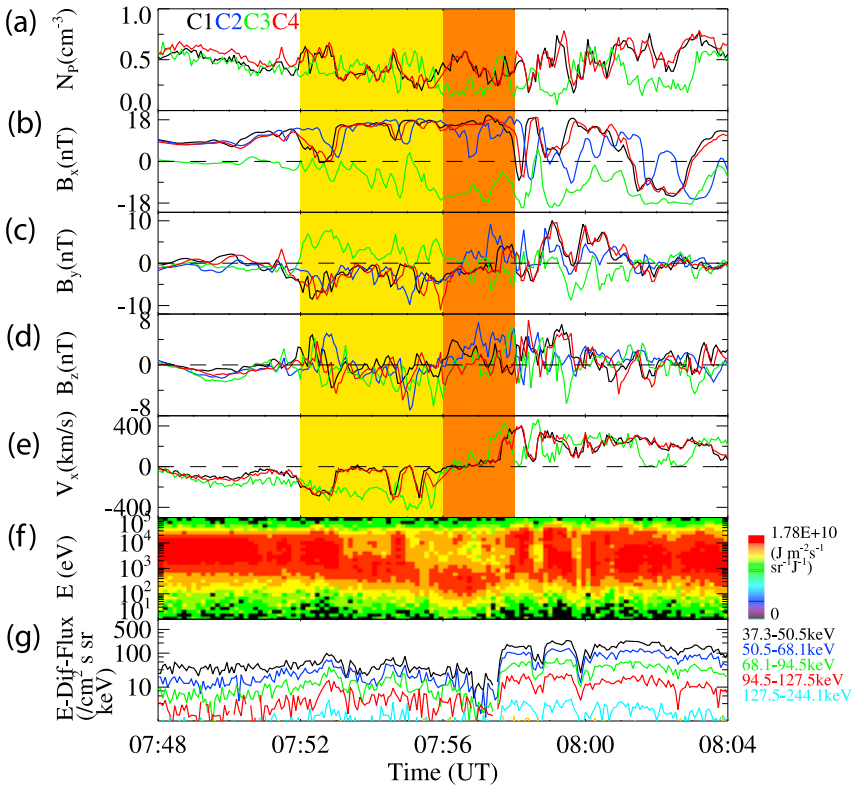


**Figure 2.** Overview of the magnetic field and ion plasma data observed by Cluster between 0748 and 0804 UT (in GSM coordinates) with a color scheme of black, blue, green, and red for spacecraft 1 to 4, respectively. (a) Proton density. (b–d) Magnetic field data and (e) $x$ component of high-speed flow. The orange and yellow vertical layers will be discussed in detail. The time resolution is 4 s. (f) Proton differential energy flux and (g) electron differential particle flux measured by the C1 satellite.

Therefore, at that time, C1, C2, and C4 stay in the upper part of the plasma sheet, and C3 is near the center of the current sheet.

[7] During the interval from 0748 to 0804 UT, there is a gradual proton flow reversal, where a tailward (negative $V_x$) high-speed flow (up to 380 km/s) is followed by an earthward (positive $V_x$) high-speed flow (up to 400 km/s) as well as an out-of-plane ($B_y$) magnetic field consistent with a Hall current. All four branches of the Hall quadrupole magnetic field are observed in this event. From about 0752 to 0756 UT, Cluster is tailward of the X line. C3 is located in the lower part of the sheet and detects positive $B_y$, while the other satellites are located in the upper part of the plasma sheet, where $B_y$ is negative. From about 0756 to 0801 UT, Cluster is earthward of the X line. C3 is located in the lower part of the plasma sheet, where $B_y$ is negative, while the other satellites are in the upper part, where $B_y$ is positive. We also find that the $z$ component of the magnetic field ($B_z$) changes from negative to positive value at 0756 UT during this reconnection event, which is coincident with the reversal of the proton flow. In addition, just before Cluster enters the ion diffusion region at about 0752 UT, $B_y$ observed by all four satellites is nearly zero. Therefore, we can conclude that Cluster passes through an ion diffusion region from tailward to earthward, and this event is an almost antiparallel reconnection without the presence of an obvious guide field. On the basis of these measurements and assuming a magnetic X line structure as a characteristic for reconnection, the approximate path of Cluster through the diffusion region can be reconstructed, as shown in Figure 3.

### 2.2. Electron Pitch Angle Distributions in the Vicinity of the X Line

[8] From about 0756 to 0758 UT (the orange region denoted in Figure 2), Cluster is in the vicinity of the X line. In Figure 4, plasma proton density (Figure 4a), the $x$ component of proton flow velocity (Figure 4e), and the three components of the magnetic field with high resolution (1/22 s) are shown. In Figure 4, the reversal of both $B_y$ and $B_z$ is clearly evidenced, indicating that Cluster is in the vicinity of the X line. Figure 5 shows the electron pitch angle distributions in the vicinity of the X line at 0756:33 UT (time a); 0756:41 UT (time b), and 0756:56 UT (time c), which are measured by C2, C1, and C4, respectively. The resolution is 4 s. Obviously, the distributions at lower energies (from 41.2 to about 923.0 eV, 40.7 to about 602.3 eV, and 41.9 to about 387.1 eV for times a, b, and c, respectively) are field-aligned bidirectional and have peaks at 0° (parallel to the magnetic field) and 180° (antiparallel to the magnetic field) and minima at 90° (perpendicular to the magnetic field). At higher energies, the distribution for time b is almost isotropic, while the distributions for times a and c have a suprathermal tail flowing along the direction antiparallel to the magnetic field. This can also be found in Figure 6, which illustrates electron distributions at times a, b, and c at the parallel (pitch angle 0°–20°), perpendicular

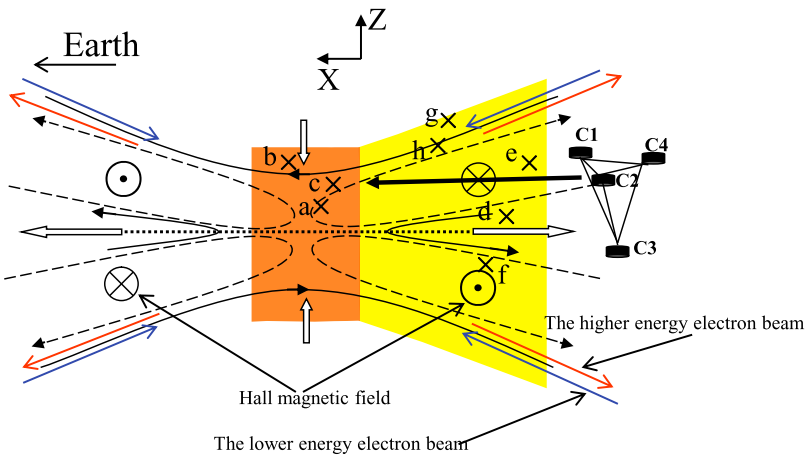


**Figure 3.** Schematic of Cluster and the geometry of the ion diffusion region in the ($X$, $Z$) plane at the beginning of the interval. The arrowed curves denote the magnetic field lines, and the dashed lines show the Hall current system. The thick arrowed curve shows the path of Cluster. The orange and yellow vertical layers correspond to the same colored layers in Figure 2. The blue and red arrows display the low-energy electron beams, flowing toward the X line region, and the high-energy electron beams, directed away from the X line, respectively.

(pitch angle 80°–100°), and antiparallel (pitch angle 160°–180°) directions. C2 at time a and C4 at time c have negative $B_y$ and positive $B_x$, and they are at the upper part of the plasma sheet and located tailward of the X line. From Figure 6, we can find that in times a and c there are more electrons streaming in the antiparallel direction than in the other two directions at higher energies. This means that the measured electron distributions have a suprathermal tail directed away from the X line. The accelerated electrons near the X line will leave this region along magnetic field lines, and these electrons cannot reach the region north of the separatrix. C2 at time a and C4 at time c measure a superthermal tail directed away from the X line, while C1 at time b does not. At the same time, C1 at time b measures larger $B_x$ (16.2 nT) than do C2 at time a (13.0 nT) and C4 at time c (16.0 nT). From Figure 1, we also find that C1 is north of C2 and C4. On the basis of this, we can conclude that times a and c are in the region south of the separatrix (in the current sheet), while time b is in the region north of the separatrix (in the lobe). The approximate positions of times a, b, and c are marked in Figure 3.

### 2.3. Electron Pitch Angle Distributions in the Outflow Region

[9] Figure 7 shows plasma proton density (Figure 7a), the $x$ component of proton flow velocity (Figure 7e), and the three components of the magnetic field (Figures 7b–7d) with high resolution (1/22 s) from 0752:00 to 0756:00 UT (the yellow region denoted in Figure 2). During this interval, both the obvious Hall term–generated $B_y$ and the $x$ component of high-speed flow can be observed, and this means that Cluster is in the outflow region. Figure 8 shows the electron pitch angle distributions at time d (0752:36 UT, measured by C4), time e (0752:37 UT, measured by C2), time f (0752:55 UT, measured by C3), time g (0755:29 UT, measured by C2), and time h (0755:49 UT, measured by C2). The resolution is 4 s. Among these five times, C2 at time g has the maximum $B_x$ value (17.8 nT), and the electron distributions are isotropic at all energies. Obviously, there are no observed suprathermal electrons, which are accelerated in the vicinity of the X line and then directed away along the magnetic field line. Therefore, we know that C2 at time g is north of the separatrix (in the lobe). At other times, we find obvious superthermal tails corresponding to the accelerated electron in the vicinity of the X line, and they are south of the separatrix (in the current sheet). Their approximate positions are marked correspondingly in Figure 3 by d, e, f, g, and h. When C2 is at time h, at lower energies, electrons stream toward the X line, while at higher energies, electrons are directed away from the X line.

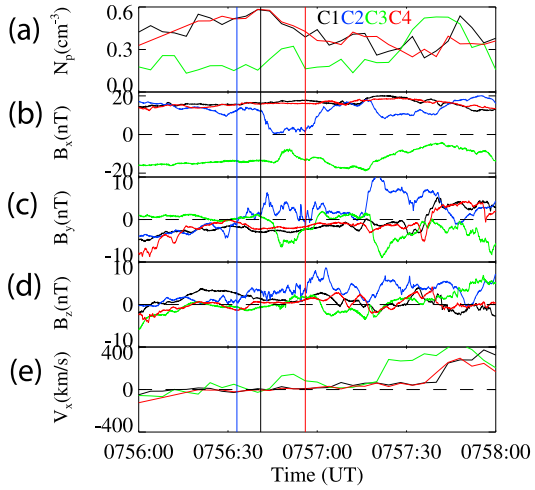


**Figure 4.** (a) Proton density, (b–d) the magnetic field data, and (e) the $x$ component of high-speed flow between 0756:00 and 0758:00 UT (in GSM coordinates). The magnetic field data have high time resolution (1/22 s). The interval corresponds to the orange region denoted in Figure 2. The vertical curves denote the time when the electron pitch angle distributions are shown in Figure 5.

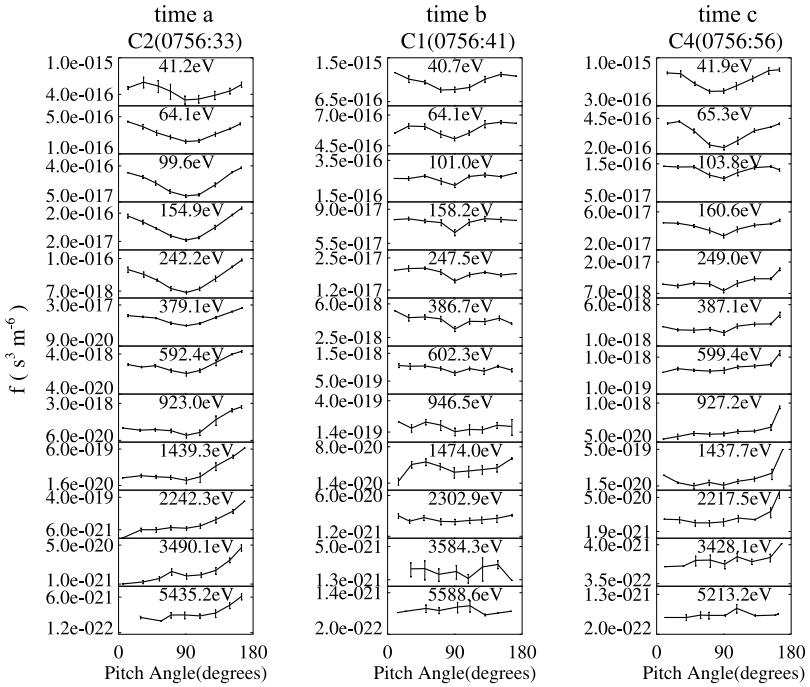


**Figure 5.** Pitch angle distribution of electrons at time a (0756:33 UT), time b (0756:41 UT), and time c (0756:56 UT) measured by C2, C1, and C4, respectively. The error bars show the standard deviation in the measurements. Cluster is in the vicinity of the X line.

The results are consistent with the observations at the edge of the outflow region by *Manapat et al.* [2006]. At the same time, $B_x$ measured by C2 at time h is about 17.0 nT, which is only slightly smaller than that measured by C2 at time g. Therefore, C2 is at the edge of the outflow region at that time. When satellites approach the center of the current sheet (C4 at time d, C2 at time e, and C3 at time f, which have smaller $B_x$ than C2 at time g), the electron distributions become field-aligned bidirectional at lower energies and isotropic at higher energies. The energy range for electron field-aligned bidirectional distributions (in this range, the electrons have field-aligned bidirectional distributions) is from 41.9 to about 1437.7 eV, 41.2 to about 5435.2eV, and 42.4 to about 1453.4 eV for C4 at time d, C2 at time e, and C3 at time f, respectively. From the observed $B_x$, we know that C4 at time d (3.9 nT) and C3 at time f (−8.8 nT) are closer to the center of the current sheet than C2 at time e (10.3 nT). Therefore, when the satellites approach the center of the current sheet, the energy range for field-aligned bidirectional distribution becomes smaller. The above results can also be found in Figure 9.

[10] We should note that in the above observational results, the resolution of the magnetic field is 1/22 s, while the resolution of the electron pitch angle distributions is 4 s. However, at the times we measure the electron pitch angle distributions, the fluctuating magnetic field at 1/22 s resolution is much smaller than its average value at 4 s resolution. Therefore, the above conclusions will not be changed if the fluctuating magnetic field is considered.

## 3. Discussion

[11] The pitch angle distributions observed in a magnetotail reconnection by Cluster can be explained by analyzing

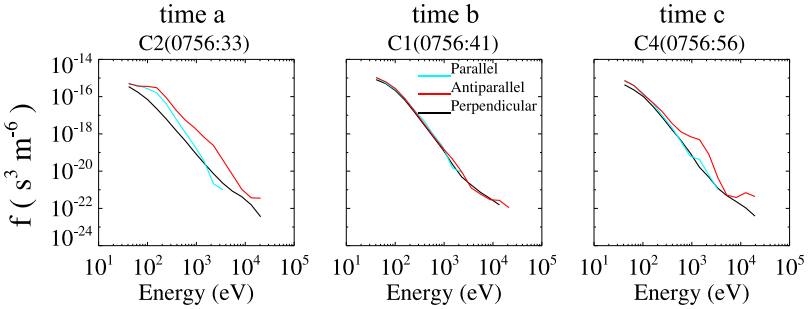


**Figure 6.** Electron distributions at time a (0756:33 UT), time b (0756:41 UT), and time c (0756:56 UT) measured by C2, C1, and C4 for parallel (pitch angle 0°−20°), antiparallel (pitch angle 160°−180°), and perpendicular (pitch angle 80°−100°) directions. Cluster is in the vicinity of the X line.

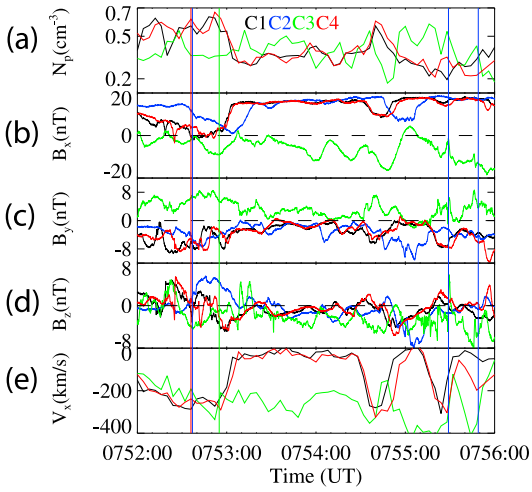


**Figure 7.** (a) Proton density, (b–d) the magnetic field data, and (e) the $x$ component of high-speed flow between 0752:00 and 0756:00 UT. The magnetic field data have high time resolution (1/22 s). The interval corresponds to the yellow region denoted in Figure 2. The vertical curves denote the time when the electron pitch angle distributions are shown in Figure 8.

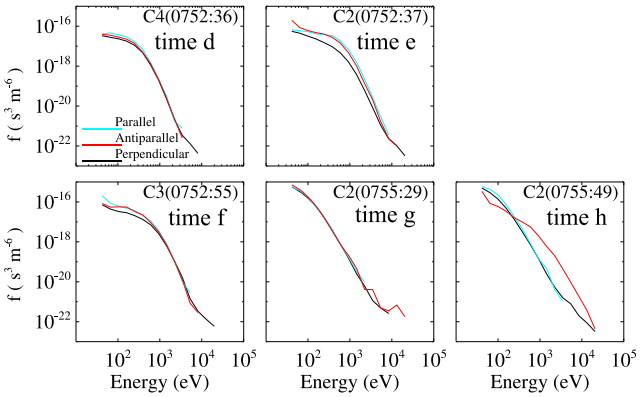


**Figure 9.** Electron distributions at time d (0752:36 UT, measured by C3), time e (0752:37 UT, measured by C2), time f (0752:55 UT, measured by C3), time g (0755:29 UT, measured by C2), and time h (0755:49 UT, measured by C2) for parallel (pitch angle 0°–20°), antiparallel (pitch angle 160°–180°), and perpendicular (pitch angle 80°–100°) directions. Cluster is in the outflow region.

typical electron trajectories in a time-stationary electric and magnetic field obtained from 2-D PIC simulations at a definite time. In the PIC simulations the electric and magnetic fields are defined on the grids and updated with a full explicit algorithm, and ions and electrons move in the electric and magnetic fields. A 1-D Harris current sheet without a guide field is chosen as our initial condition. The corresponding magnetic field and density are described as

$$\mathbf{B}_0(z) = B_0 \tanh(z/\delta)\mathbf{e}_x, n(z) = n_0 \mathrm{sech}^2(z/\delta) + n_b.$$

The density has two parts: the first part corresponds to the Harris density, while the other part corresponds to the

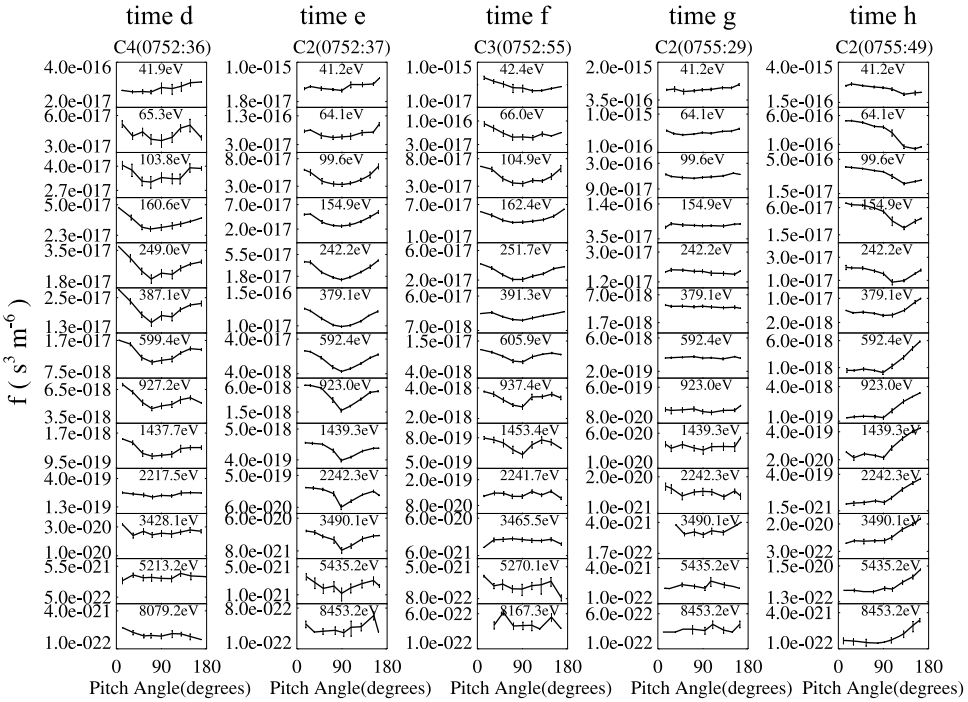


**Figure 8.** Electron pitch angle distributions at time d (0752:36 UT, measured by C4), time e (0752:37 UT, measured by C2), time f (0752:55 UT, measured by C3), time g (0755:29 UT, measured by C2), and time h (0755:49 UT, measured by C2). The error bars show the standard deviation in the measurements. Cluster is in the outflow region.

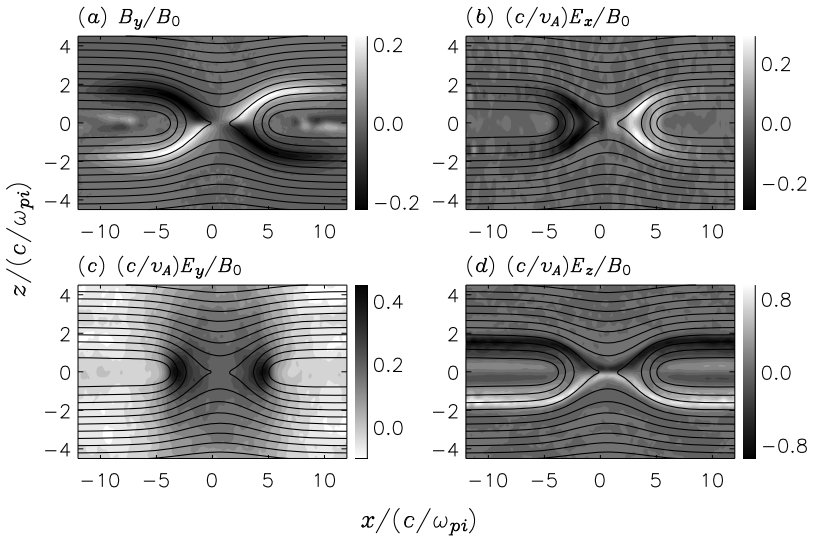


**Figure 10.** Contours of (a) $B_y/B_0$, (b) $(c/v_A)E_x/B_0$, (c) $(c/v_A)E_y/B_0$, and (d) $(c/v_A)E_z/B_0$ at $\Omega_i t = 21$. The in-plane magnetic field lines at $\Omega_i t = 21$ are also presented.

background density. Here $n_0$ and $n_b$ represent the peak Harris and background densities, respectively, and $\delta$ is the half width of the current sheet, which is chosen as $\delta = 0.5c/\omega_{pi}$ (where $c/\omega_{pi}$ is the ion inertial length defined with the peak Harris density $n_0$). The ion-to-electron mass ratio is $m_i/m_e = 100$, and $c = 15v_A$ (where $v_A$ is the Alfvén speed based on the asymptotic magnetic field $B_0$ and $n_0$). The initial ion-to-electron temperature ratio is $T_{i0}/T_{e0} = 5$ and $n_b = 0.2n_0$. The particles are assumed to satisfy Maxwellian distributions. The particles corresponding to the Harris current have a drift speed along the $y$ direction, while the background particles have no drift speed. The computation is carried out in the rectangular domain with dimension $L_x \times L_z = (25.6c/\omega_{pi}) \times (12.8c/\omega_{pi})$, and the spatial resolution is $\Delta x = \Delta z = 0.05c/\omega_{pi}$. The time step is $\Omega_i t = 0.001$, where $\Omega_i = q_i B_0/m_i$ is the ion cyclotron frequency. In order to put the system in the nonlinear regime from the beginning of the simulation, an initial flux perturbation is introduced. All the parameters and the periodic boundary conditions are the same as in the Geospace Environmental Modeling magnetic reconnection challenge [*Birn et al.*, 2001], except that we use a larger ion-to-electron ratio, $m_i/m_e = 100$.

[12] Because of the limitations of the PIC simulations, like the periodic boundary conditions, and the limited domain size, it is difficult to maintain a quasi-stationary reconnection rate and follow the trajectories of electrons with very high energy. Therefore, we cannot reproduce all the observed results in simulations. However, we still can deduce the observed results by ray tracing several typical electrons. The electric and magnetic fields of the reconnection at $\Omega_i t = 21$ were chosen for ray tracing electrons. This corresponds to the time when the reconnection rate was a maximum during the simulation. Two typical electron trajectories are then traced in this simulation structure. Figure 10 illustrates the out-of-plane magnetic field $B_y/B_0$ (Figure 10a), the electric field in the $x$ direction $(c/v_A)E_x/B_0$ (Figure 10b), the electric field in the $y$ direction $(c/v_A)E_y/B_0$ (Figure 10c), and the electric field in the $z$ direction $(c/v_A)E_z/B_0$ at $\Omega_i t = 21$ (Figure 10d). The magnetic field lines at $\Omega_i t = 21$ are also presented in Figure 10. The maximum island half width is about $2.0c/\omega_{pi}$. The reconnection electric field $E_y$ can be found in the vicinity of the X line, and the out-of-plane magnetic field $B_y$ has a quadrupole structure. $E_x$ forms a bicrescent shape symmetric around the X line with a negative value in region $x < 0$ and a positive value in region $x > 0$, while $E_z$ forms two strips symmetric along $z = 0$ with a positive value in region $z < 0$ and a negative value in region $z > 0$.

[13] Figure 11 depicts the two typical electron trajectories that pass through the vicinity of the X line. In Figure 11, the magnetic field lines at $\Omega_i t = 21$ are presented for reference.

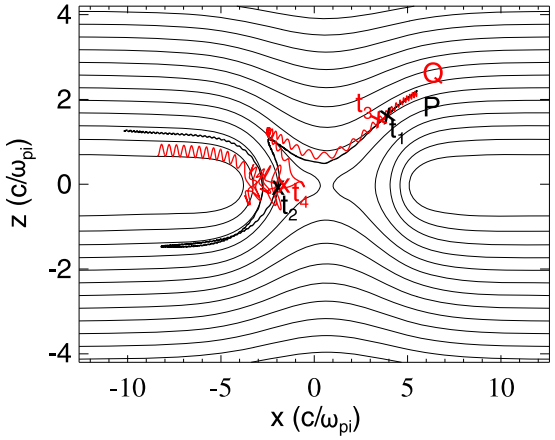


**Figure 11.** Two typical electron trajectories passing through the X-type region. The in-plane magnetic field lines at $\Omega_i t = 21$ are also presented. Initially, both particles are at $(x, z) = (5.5c/\omega_{pi}, 2.3c/\omega_{pi})$, and their energies $\varepsilon = 1/2m_e v^2$ are $0.125m_e v_A^2$ (denoted by P) and $22.2m_e v_A^2$ (denoted by Q), respectively. The time interval between $t_1$ and $t_2$ represents the time period during which the electron P is in the vicinity of the X line, while the interval between $t_3$ and $t_4$ represents the time period during which the electron Q is in the vicinity of the X line.

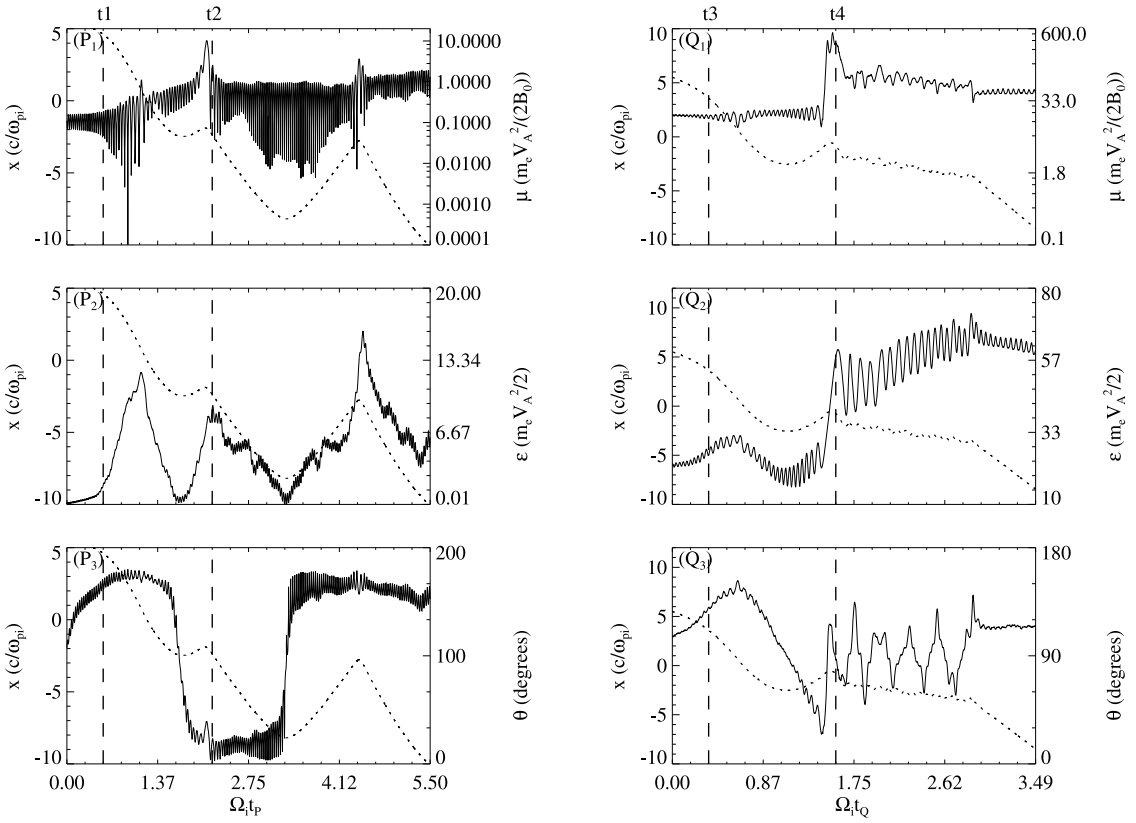


**Figure 12.** Evolution of the magnetic moment $\mu$ (= $m_e v_\perp^2/(2B)$), energy $\varepsilon$, and pitch angle of the electrons. (left) The particle P: P1, P2, and P3 denote the magnetic moment $\mu$ (= $m_e v_\perp^2/(2B)$), energy $\varepsilon$, and pitch angle, respectively. (right) The particle Q: Q1, Q2, and Q3 denote the magnetic moment $\mu$ (= $m_e v_\perp^2/(2B)$), energy $\varepsilon$, and pitch angle, respectively. Variables $t_P$ and $t_Q$ are measured from the time $\Omega_i t$ = 21, when the stationary electric and magnetic fields of the reconnection are chosen.

Initially, both electrons are at ($x$, $z$) = ($5.5c/\omega_{pi}$, $2.3c/\omega_{pi}$), and their energies $\varepsilon = 1/2 m_e v^2$ are $0.125 m_e v_A^2$ (denoted by P in Figure 11) and $22.2 m_e v_A^2$ (denoted by Q in Figure 11), respectively. They are north of the separatrix and outside of the ion diffusion region (in the lobe). The evolution of the magnetic moment $\mu$ (= $m_e v_\perp^2/(2B)$), energy $\varepsilon$, and pitch angle of the electrons are depicted in Figure 12. Figure 12 (left) illustrates the particle P, and Figure 12 (right) depicts the particle Q. At first, the electrons move toward the X line almost along the magnetic field lines. The motions of the electrons are nearly adiabatic ($\mu$ = $m_e v_\perp^2/(2B)$ is almost constant) until they reach the vicinity of the X line. When they move toward the X line because of the weak magnetic field in the vicinity of the X line, the perpendicular velocities of the electrons decrease, and their parallel velocities increase. Therefore, their pitch angles approach 180° during this period. The electrons may bounce several times almost along the magnetic field lines due to the magnetic mirror. At the same time, they achieve a velocity in the $-z$ direction due to $\mathbf{E} \times \mathbf{B}$ drift in the vicinity of the X line ($\mathbf{E}$ has a component in the $y$ direction in the vicinity), and the electrons go to the south of the separatrix (in the current sheet). In the vicinity of the X line, the motions of the electrons are nonadiabatic. The electrons are accelerated by the reconnection electric field to higher energy in the vicinity of the X line and then leave along the magnetic field lines (the pitch angles are near 0°). In the vicinity of the X line, the electrons at lower energies flow toward the X line and then may be bounced along the magnetic field lines by the magnetic mirror, which forms the observed field-aligned bidirectional distributions, while the electrons at higher energies have gyroradii comparable to the curvature radii of the magnetic field lines, and their motions are stochastic, which forms the observed isotropic distributions in the region north of the separatrix [*Chen and Palmadesso*, 1986]. Because of the limitation of our simulation domain and the reduced light speed, it is difficult to follow the trajectories of the electrons with very high energy. In the region south of the separatrix (in the current sheet), the energetic electrons stream away from the X line along the magnetic field lines after being accelerated by the reconnection electric field near the X line, and they form the high-energy tail directed away from the X line in the observations.

[14] After the accelerated electrons enter the outflow region, the electrons with lower energies are magnetically mirrored because of the strong magnetic field in the outflow region and may bounce several times. For low-energy particles (particle P), in most regions, the pitch angle is near 0° or 180°, except at the turning points, and we observe the field-aligned bidirectional distributions at low energies. The electrons at higher energies (particle Q) have larger gyroradii, and their motions become stochastic when their radii are comparable to the curvature radii of the magnetic field lines. The pitch angle changes rapidly. In this way,

isotropic distributions can be formed. The energy threshold from the bidirectional to isotropic distributions depends on the amplitude and topology of the magnetic field. When Cluster approaches the center of the current sheet, the electron gyroradii become large with the decrease of the magnetic field; simultaneously, the curvature radii of the magnetic field lines become small. Therefore, the motions of the electrons easily become stochastic and form isotropic distributions, which is consistent with the observed pitch angle distributions in the outflow region by Cluster. At the edge of the outflow region, the magnetic field is very strong, and the electron gyroradii are small. At the same time, the curvature radii of the magnetic field lines are large, and isotropic distributions are difficult to observe. Therefore, we can observe the electrons with higher energy directed away from the X line at the edge of the outflow region. In reality, assuming that an electron has 6000 eV and that its speed is about $0.15c$, its gyroradius is about $0.15c\Omega_e^{-1}$. According to the observed magnetic field (about 5 nT) and density ($1.0\ \mathrm{cm}^{-3}$), we can calculate $\Omega_e^{-1} \approx 64\omega_{pe}^{-1} \approx 1.5\omega_{pi}^{-1}$ ($m_i/m_e$ is assumed to be 1836), and the gyroradius is about $0.23c/\omega_{pi}$. Therefore, the gyroradius of the electron is comparable to the half width of the current sheet. Considering that the curvature radii of the magnetic field lines change largely in different regions, the motions of electrons at higher energies may be stochastic in some regions of the magnetotail reconnection.

[15] The electron pitch angle distributions in a deep-tail reconnection event have also been observed by the Wind spacecraft [*Øieroset et al.*, 2002], and the electron distributions in the vicinity of the X line are also found to be field-aligned bidirectional at lower energies and isotropic at higher energies. The reconnection event has a very strong guide field, which is comparable to the asymptotic magnetic field $B_0$. *Egedal et al.* [2005] found that the strong electrostatic potential in the vicinity of the X line plays a key role in trapping electrons and forms such anisotropic distributions. Different from their case, in our observations, there is no obvious guide field, and we found that such anisotropic distributions can be observed not only in the vicinity of the X line, but also in the outflow region. The generation mechanisms of such electron distributions are also different from that described by *Egedal et al.* [2005].

## 4. Conclusions

[16] In this paper, we presented Cluster observations of a magnetotail reconnection event without an obvious guide field and analyzed the electron pitch angle distributions in the vicinity of the X line and the outflow region. In the vicinity of the X line, at lower energies, the electron distributions are field-aligned bidirectional, and a high-speed stream directed away from the X line inside the ion diffusion region is observed. The bidirectional distributions at lower energies are the result of a magnetic mirror in the reconnections, and the acceleration by the reconnection electric field near the X line leads to a high-speed stream away from the X line. At the edge of the outflow region, there is a high-speed electron stream directed away from the X line and a low-speed stream directed toward the X line, which has also been observed previously in the magnetotail [*Fujimoto et al.*, 1997; *Nagai et al.*, 2001; *Alexeev et al.*, 2005; *Manapat et al.*, 2006]. When Cluster approaches the center of the current sheet, the distributions become field-aligned bidirectional at lower energies and isotropic at higher energies. The electrons at lower energies are magnetically mirrored, and they may bounce along the magnetic field lines several times, forming the field-aligned directional distributions. At higher energies, the radii of the electrons become large and comparable to the curvature radii of the magnetic field lines, and their motions become stochastic, forming isotropic distributions. The energy threshold from the bidirectional to isotropic distributions depends on the amplitude and topology of the magnetic field. At the edge of the outflow region, where the amplitude of the magnetic field is strong and the curvature radii of the magnetic field lines become large, the electron motions do not easily become stochastic. Therefore, isotropic distributions at the edge of the outflow region cannot be observed.

[17] **Acknowledgments.** This research was supported by the Chinese Academy of Sciences under grant KJCX2-YW-N28; the National Science Foundation of China (NSFC) under grants 40674093, 40725013, and 40874075; and the Specialized Research Fund for State Key Laboratories. R. Wang acknowledges helpful discussion with Andrew Fazakerley at University College London. All Cluster data are obtained from the ESA Cluster Active Archive. We thank the FGM, CIS, PEACE, and EFW instrument teams and the ESA Cluster Active Archive.

[18] Amitava Bhattacharjee thanks the reviewers for their assistance in evaluating this paper.

## References

Alexeev, I. V., C. J. Owen, A. N. Fazakerley, A. Runov, J. P. Dewhrst, A. Balogh, H. Rème, B. Klecker, and L. Kistler (2005), Cluster observations of currents in the plasma sheet during reconnection, *Geophys. Res. Lett.*, *32*, L03101, doi:10.1029/2004GL021420.

Asnes, A., M. G. G. T. Taylor, A. L. Borg, B. Lavraud, R. W. H. Friedel, C. P. Escoubet, H. Laakso, P. Daly, and A. N. Fazakerley (2008), Multispacecraft observation of electron beam in reconnection region, *J. Geophys. Res.*, *113*, A07S30, doi:10.1029/2007JA012770.

Balogh, A., et al. (2001), The Cluster magnetic field investigation: Overview of in-flight performance and initial results, *Ann. Geophys.*, *19*, 1207–1217.

Birn, J., et al. (2001), Geospace Environmental Modeling (GEM) magnetic reconnection challenge, *J. Geophys. Res.*, *106*, 3715–3719.

Biskamp, D. (2000), *Magnetic Reconnection in Plasma*, Cambridge Univ. Press, Cambridge, U. K.

Cai, H. J., and L. C. Lee (1997), The generalized Ohm's law in collisionless magnetic reconnection, *Phys. Plasmas*, *4*, 509–520.

Cao, J. B., et al. (2006), Joint observations by Cluster satellites of bursty bulk flows in the magnetotail, *J. Geophys. Res.*, *111*, A04206, doi:10.1029/2005JA011322.

Chen, J., and P. J. Palmadesso (1986), Chaos and nonlinear dynamics of single-particle orbits in a magnetotaillike magnetic field, *J. Geophys. Res.*, *91*, 1499–1508.

Chen, L. J., et al. (2008a), Observation of energetic electrons within magnetic islands, *Nat. Phys.*, *4*, 19–23.

Chen, L. J., et al. (2008b), Evidence of an extended electron current and its neighboring magnetic island during magnetotail reconnection, *J. Geophys. Res.*, *113*, A12213, doi:10.1029/2008JA013385.

Deeg, H. J., J. E. Borovsky, and N. Duric (1991), Particle acceleration near X-type magnetic neutral lines, *Phys. Fluids B*, *3*, 2660–2674.

Drake, J. F., M. A. Shay, and M. Swisdak (2008), The Hall fields and fast magnetic reconnection, *Phys. Plasma*, *15*, 042306.

Egedal, J., M. Øieroset, W. Fox, and R. P. Lin (2005), In situ discovery of an electrostatic potential, trapping electrons and mediating fast reconnection in the Earth's magnetotail, *Phys. Rev. Lett.*, *94*, 025006.

Escoubet, C., M. Fehringer, and M. Goldstein (2001), The Cluster mission, *Ann. Geophys.*, *19*, 1197–1200.

Fu, X. R., Q. M. Lu, and S. Wang (2006), The process of electron acceleration during collisionless magnetic reconnection, *Phys. Plasmas*, *13*, 012309.

Fujimoto, M., M. S. Nakamura, I. Shinohara, T. Nagai, T. Mukai, Y. Saito, T. Yamamoto, and S. Kokubun (1997), Observations of earthward streaming electrons at the trailing boundary of a plasmoid, *Geophys. Res. Lett.*, *24*, 2893–2896.

Ge, Y. S., and C. T. Russell (2006), Polar survey of magnetic field in near tail: Reconnection rare inside 9 $R_E$, *Geophys. Res. Lett.*, *33*, L02101, doi:10.1029/2005GL024574.

Giovanelli, R. G. (1946), A theory of chromospheric flares, *Nature*, *158*, 81–82.

Hesse, M., and D. Winske (1998), Electron dissipation in collisionless magnetic reconnection, *J. Geophys. Res.*, *103*, 26,479–26,486.

Hesse, M., M. Kuznetsova, and J. Birn (2001), Particle-in-cell simulations of three-dimensional collisionless magnetic reconnection, *J. Geophys. Res.*, *106*, 29,831–29,841.

Hoshino, H., T. Mukai, T. Terasawa, and I. Shinohara (2001), Suprathermal electron acceleration in magnetic reconnection, *J. Geophys. Res.*, *106*, 25,979–25,997.

Imada, S., R. Nakamura, P. W. Daly, M. Hoshino, W. Baumjohann, S. Muhlbachler, A. Balogh, and H. Reme (2007), Energetic electron acceleration in the downstream reconnection outflow region, *J. Geophys. Res.*, *112*, A03202, doi:10.1029/2006JA011847.

Johnstone, A. D. (1997), PEACE: A Plasma Electron and Current Experiment, *Space Sci. Rev.*, *79*, 351–398.

Kuznetsova, M., M. Hesse, and D. Winske (2001), Collisionless reconnection supported by nongyrotropic pressure effects in hybrid and particle simulations, *J. Geophys. Res.*, *106*, 3799–3810.

Lin, R. P., and H. S. Hudson (1976), Non-thermal process in large solar flares, *Sol. Phys.*, *50*, 153–178.

Litvinenko, Y. E. (1996), Particle acceleration in reconnecting current sheets with a nonzero magnetic field, *Astrophys. J.*, *462*, 997–1004.

Ma, Z. W., and A. Bhattacharjee (2001), Hall magnetohydrodynamic reconnection: The Geospace Environment Modeling challenge, *J. Geophys. Res.*, *106*, 3773–3782.

Manapat, M., M. Øieroset, T. D. Phan, R. P. Lin, and M. Fujimoto (2006), Field-aligned electrons at the lobe/plasma sheet boundary in the mid-to-distant magnetotail and their association with reconnection, *Geophys. Res. Lett.*, *33*, L05101, doi:10.1029/2005GL024971.

McPherron, R. L., A. Nishida, and C. T. Russell (1987), Is near-Earth current sheet thinning the cause of auroral substorm onset?, in *Quantitative Modeling of Magnetosphere-Ionosphere Coupling Processes*, edited by Y. Kamide and R. A. Wolf, pp. 252–257, Kyoto Sangyo Univ., Kyoto, Japan.

Miller, J. A., P. J. Cargill, A. Emslie, G. D. Holamn, B. R. Dennis, T. N. Larosa, R. M. Winglee, S. G. Benka, and S. Tsuneta (1997), Critical issues for understanding particle acceleration in impulsive solar flares, *J. Geophys. Res.*, *102*, 14,631–14,659.

Nagai, T., I. Shinohara, M. Fujimoto, M. Hoshino, Y. Saito, S. Machida, and T. Mukai (2001), Geotail observations of the Hall current system: Evidence of magnetic reconnection in the magnetotail, *J. Geophys. Res.*, *106*, 25,929–25,949.

Nagai, T., I. Shinohara, M. Fujimoto, S. Machida, R. Nakamura, Y. Saito, and T. Mukai (2003), Structure of the Hall current system in the vicinity of the magnetic reconnection site, *J. Geophys. Res.*, *108*(A10), 1357, doi:10.1029/2003JA009900.

Nishida, A. (1978), *Geomagnetic Diagnostics of the Magnetosphere*, Springer, New York.

Øieroset, M., T. D. Phan, M. Fujimoto, R. P. Lin, and R. P. Lepping (2001), In situ detection of collisionless reconnection in the Earth's magnetotail, *Nature*, *412*, 414–417.

Øieroset, M., R. P. Lin, T. D. Phan, D. E. Larson, and S. D. Bale (2002), Evidence for electron acceleration up to ~300 keV in the magnetic reconnection diffusion region of Earth's magnetotail, *Phys. Rev. Lett.*, *89*, 195001, doi:10.1103/PhysRevLett.89.195001.

Parker, E. (1957), Sweet's mechanism for merging magnetic fields in conducting fluids, *J. Geophys. Res.*, *62*, 509–520.

Priest, E., and T. Forbes (2000), *Magnetic Reconnection: MHD Theory and Applications*, Cambridge Univ. Press, Cambridge, U. K.

Pritchett, P. L. (2001), Geospace Environment Modeling magnetic reconnection challenge: Simulations with a full particle electromagnetic code, *J. Geophys. Res.*, *106*, 3783–3798.

Pritchett, P. L. (2006a), Relativistic electron production during driven magnetic reconnection, *Geophys. Res. Lett.*, *33*, L13104, doi:10.1029/2005GL025267.

Pritchett, P. L. (2006b), Relativistic electron production during guide field magnetic reconnection, *J. Geophys. Res.*, *111*, A10212, doi:10.1029/2006JA011793.

Pritchett, P. L., and F. V. Coroniti (2004), Three-dimensional collisionless magnetic reconnection in the presence of a guide field, *J. Geophys. Res.*, *109*, A01220, doi:10.1029/2003JA009999.

Rème, H., et al. (2001), First multispacecraft ion measurements in and near the Earth's magnetosphere with the identical Cluster ion spectrometry (CIS) experiment, *Ann. Geophys.*, *19*, 1303–1354.

Retino, A., et al. (2006), Structure of the separatrix region close to a magnetic reconnection X-line: Cluster observations, *Geophys. Res. Lett.*, *33*, L06101, doi:10.1029/2005GL024650.

Retino, A., et al. (2008), Cluster observations of energetic electrons and electromagnetic fields with a reconnecting thin current sheet in the Earth's magnetotail, *J. Geophys. Res.*, *113*, A12215, doi:10.1029/2008JA013511.

Scudder, J. D., F. S. Mozer, N. C. Maynard, and C. T. Russell (2002), Fingerprints of collisionless reconnection at the separator: I. Ambipolar-Hall signatures, *J. Geophys. Res.*, *107*(A10), 1294, doi:10.1029/2001JA000126.

Sergeev, V., et al. (2008), Study of near-Earth reconnection events with Cluster and Double Star, *J. Geophys. Res.*, *113*, A07S36, doi:10.1029/2007JA012902.

Shay, M. A., J. F. Drake, B. N. Rogers, and R. E. Denton (2001), Alfvénic collisionless magnetic reconnection and the Hall term, *J. Geophys. Res.*, *106*, 3759–3772.

Speiser, T. W. (1965), Particle trajectories in a model current sheet, based on the open model of the magnetosphere, with applications to auroral particles, *J. Geophys. Res.*, *70*, 1717–1728.

Sweet, P. A. (1958), The neutral point theory of solar flare, in *Electromagnetic Phenomena in Cosmical Physics*, edited by B. Lehrert, p. 123, Cambridge Univ. Press, London.

Tsuneta, S., H. Hara, T. Shimizu, L. W. Acton, K. T. Strong, H. S. Hudson, and Y. Ogawara (1992), Observation of a solar flare at the limb with the Yohkoh Soft X-ray Telescope, *Publ. Astron. Soc. Jpn.*, *44*, L63–L69.

Vasyliunas, V. M. (1975), Theoretical models of magnetic field line merging, *Rev. Geophys. Space Phys.*, *13*, 303–336.

Wan, W. G., and G. Lapenta (2008), Electron self-reinforcing process of magnetic reconnection, *Phys. Rev. Lett.*, *101*, 015001.

Wan, W. G., G. Lapenta, G. L. Delzanno, and J. Egedal (2008), Electron acceleration during guild field magnetic reconnection, *Phys. Plasmas*, *15*, 032903.

Wang, R. S., Q. M. Lu, J. Guo, and S. Wang (2008), Spatial distribution of energetic electrons during magnetic reconnection, *Chin. Phys. Lett.*, *25*, 3083–3085.

Wang, X., A. Bhattacharjee, and Z. W. Ma (2001), Scaling of collisionless forced reconnection, *Phys. Rev. Lett.*, *87*, 265003.

Wei, X. H., J. B. Cao, G. C. Zhou, O. Santolík, H. Rème, I. Dandouras, N. Cornilleau-Wehrlin, E. Lucek, C. M. Carr, and A. Fazakerley (2007), Cluster observations of waves in the whistler frequency range associated with magnetic reconnection in the Earth's magnetotail, *J. Geophys. Res.*, *112*, A10225, doi:10.1029/2006JA011771.

Wesson, J. (1997), *Tokomaks*, Oxford Univ. Press, New York.

Xiao, C. J., et al. (2007), Cluster measurements of fast magnetic reconnection in the magnetotail, *Geophys. Res. Lett.*, *34*, L01101, doi:10.1029/2006GL028006.

Zong, Q. G., et al. (2004), Cluster observations of earthward flowing plasmoid in the tail, *Geophys. Res. Lett.*, *31*, L18803, doi:10.1029/2004GL020692.

C. Huang, Q. Lu, R. Wang, and S. Wang, Chinese Academy of Sciences Key Laboratory of Basic Plasma Physics, School of Earth and Space Sciences, University of Science and Technology of China, 96 JinZhai Rd., Hefei, Anhui 230026, China. (qmlu@ustc.edu.cn)